Ultrafast dynamics of three types of simultaneous shockwaves and filament attenuation in femtosecond laser multi-pulse ablation of PMMA

Guoyan Wang (王国燕)[1], Lan Jiang (姜 澜)[1], Jingya Sun (孙靖雅)[1], Jie Hu (胡 洁)[1,*], Qingsong Wang (王青松)[1], Ming Li (李 明)[2], and Yongfeng Lu (陆永枫)[3]

[1]*Laser Micro/Nano Fabrication Laboratory, School of Mechanical Engineering, Beijing Institute of Technology, Beijing 100081, China*
[2]*Xi'an Institute of Optics and Precision Mechanics, Chinese Academy of Sciences, Xi'an 710119, China*
[3]*Department of Electrical Engineering, University of Nebraska-Lincoln, Lincoln, Nebraska 68588-0511, USA*
Corresponding author: jiehu2@bit.edu.cn

Cylindrical shockwaves inside polymethyl methacrylate (PMMA) generated simultaneously with two hemispherical shockwaves induced by a femtosecond Gaussian beam laser were investigated using an ultrafast pump–probe imaging technique. The evolutions of these three shockwaves with probe delay and incident pulse number have been systematically analyzed. The plasma intensity and filament length in the center of cylindrical shockwave both decayed with pulse number. Moreover, the self-focused filament moved downstream towards the output surface with an increased pulse number. The experimental results and mechanism illustrated that energy deposition was suppressed by a degraded nonlinear effect due to a pre-ablated structure in multi-pulse irradiation.

OCIS codes: 140.7090, 320.7120, 350.5400, 350.3390.
doi: 10.3788/COL201917.081405.

In recent years, three-dimensional (3D) micro/nano structures fabricated in transparent materials, such as waveguides[1], gratings[2], microholes[3], optical memories[4], and microfluidic devices[5], have received extensive attention. Compared with glass, polymethyl methacrylate (PMMA) has unique advantages in applications because of its low cost, easy machining, and high transmission in the visible region. The high precision and reduced heat-affected zone of the femtosecond (fs) laser[6,7] are ideal for satisfying the increased quality requirements in PMMA devices. Zhang *et al.*[8] realized microhole fabrication in polymers with an aspect ratio of 10:1 using 100 fs laser pulses. Chu *et al.* increased the ablation efficiency of microholes by a factor of 3 using a defocused irradiation assisted fs laser[9]. Liu *et al.*[10] improved the machining efficiency by dividing 800 nm fs laser pulses into a double pulses train with pulse delays shorter than 1 ps. It was also found that the etching depth of the microchannel can be improved by a fs laser pulse train[11]. Xie *et al.* upgraded the aspect ratio of the microchannel to 330:1 using a spatially shaped single Bessel fs laser pulse[12]. Moreover, the properties of the material can be influenced by the nonlinear propagation/absorption of fs laser pulses[13]. Utilizing this technique, refractive index changes and voids have also been induced inside PMMA with fs laser multiple pulses[14]. However, the material response and laser energy deposition mechanism of multiple pulses irradiation is different from that of single pulse irradiation of a flat surface and is influenced by the pre-pulses ablated structures[15]. Wang *et al.* have reported that the plasma dynamics in

multiple pulses irradiation of fused silica was enhanced by a pre-pulse ablated crater with ultrafast pump–probe shadowgraphs[16]. Although series studies have been undertaken to investigate the morphology or structure evolution during multiple pulses ablation of PMMA, very few pump–probe studies have been carried out concerning the ultrafast dynamics of plasma/shockwaves induced by multiple pulses. The fundamental mechanism of multiple pulses manufacturing remains mysterious, and revelations of the ultrafast dynamics and energy deposition mechanism of the multiple pulses process are of urgent need.

In this Letter, an ultrafast pump–probe shadowgraph imaging technique was applied to detect the plasma and shockwave dynamics during a sequence of fs laser pulse interaction with PMMA. Benefiting from the transparency of PMMA, plasma and shockwaves both inside and outside the sample can be simultaneously recorded and discussed. In past papers, hemispherical shockwaves (HSWs) and cylindrical shockwaves (CSWs) were not induced inside PMMA simultaneously when a Gaussian beam was focused on the surface[17]. However, three types of shockwaves were observed simultaneously after fs pulses irradiation that evolved with the number of incident laser pulses. HSW1 outside the sample decayed with pulse number and was affected by the structure induced by the previous pulses. An unexpected CSW was discovered deep below the PMMA surface with HSW2 propagating under the shallow surface. A CSW, as reported, can be induced when a Gaussian beam is focused inside the material or with Bessel beam ablation. In the case of

Gaussian beam focusing on the surface of PMMA, the generation of a CSW indicated that laser energy of a Gaussian beam can be deposited deep into the sample beyond the Rayleigh length by laser-induced filaments (FLs). In other words, FLs can also be induced, except for laser focusing inside material. The mechanism of filamentation in condition of laser pulse focus on the surface was attributed to the nonlinear effect. A radial refractive index gradient around the surface induced by the nonlinear effect resulted in the focusing of a laser beam in a linear range in PMMA. The FL moved downstream and degenerated with increasing numbers of laser pulses. The structure ablated by the preceding pulses strongly affected the laser intensity field distribution and energy deposition of subsequent pulses.

The experimental setup is illustrated in detail in Fig. 1. A regenerative amplified Ti:sapphire laser system (Spectra Physics, Inc.) with central wavelength of 800 nm and full width at half-maximum (FWHM) of 50 fs was applied to generate Gaussian fs laser pulses. The fs laser beam was divided into pump and probe beams by a beam splitter (BS). The PMMA sample (10 mm × 10 mm × 1 mm, double polished, Hefei Kejing) was perpendicularly fixed on the motorized translation stage. Pulse energy was adjusted by a continuous attenuator. The combination of a half-wave plate and polarizer was another complementary method for energy adjustment. The pump pulse was perpendicularly focused on the side plane (home polished) of the sample by a five times objective lens (NA = 0.15, Olympus). The probe pulse was frequency doubled by a beta barium borate (BBO) crystal and then irradiated on the front side of the sample orthogonally. The transmitted probe beam was recorded by a charge-coupled device (CCD) camera through a 20 times objective lens (NA = 0.45, Olympus). A 400 nm bandpass filter was set before the CCD camera to restrict the residual 800 nm wavelength and the fluorescence radiation of plasma. The time delay between the pump and probe pulses was controlled by an optical delay line. The focus diameter of the pump pulse was about 10 μm. A homemade synchronous trigger was used to control the timing sequence of the export of laser pulses and the exposure of the CCD camera.
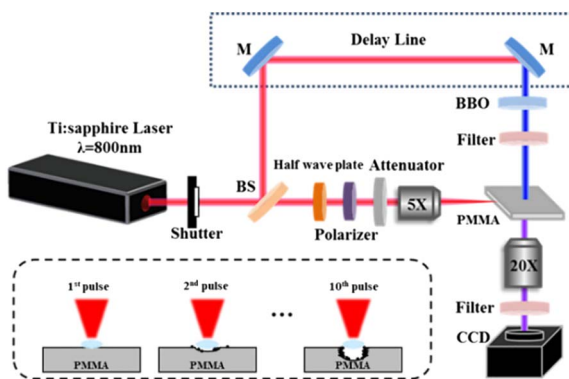
In order to study the ablation dynamics with series of pulses, the sample was not shifted to a fresh point until images were recorded for each pulse. To improve the signal to noise ratio, every shadowgraph was subtracted by a background image.

In our experiments, 10 fs laser pulses were applied to illuminate the sample at the same position to investigate the ablation dynamics of multiple pulses irradiation. The laser was set in the mode of gated to export a single pulse at one time for each round of shadowgraph capturing, and the time interval between pulses was more than 1 s. The sample was moved to a fresh point after 10 pulses for another circulation. Figure 2 shows the shadowgraph after the first pulse ablation of PMMA at a probe delay of 16 ns. The laser pulse irradiated the surface from the left with a perpendicular incidence angle. With laser fluence of more than 8 J/cm², only HSW1 outside the material and HSW2 inside the material were detectable in our imaging system. When laser fluence increased to 11.9 J/cm², three shockwaves, namely HSW1, HSW2, and the unexpected CSW inside the material, were generated simultaneously by a single fs laser pulse, as shown in Fig. 2. The three shockwaves also can be induced simultaneously with higher laser fluence, and the morphologies of HSW2 and CSW were unchanged except for a bulge of HSW1 in the Z direction induced by air breakdown with a large laser fluence. However, in previous studies, only HSW1 and HSW2 were induced when a Gaussian beam focused on the surface of sample[17], and CSW was generated individually in Bessel beam ablation due to its long Rayleigh length[18]. The CSW induced in this study revealed that pulse energy of a Gaussian beam can be deposited deeply into the material beyond the Rayleigh length. It was the first time that a CSW existed together with HSW1 and HSW2 in Gaussian beam ablation, to the best of our knowledge. When the fs laser pulse irradiated the surface, multi-photon absorption of the pulse energy occurred immediately. Plasma induced by intense ionization was excited closely near the surface with a sharp increase in

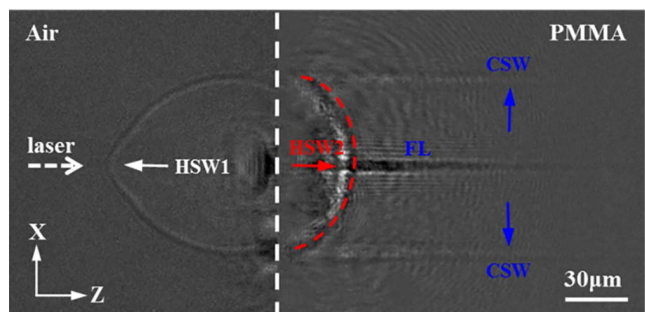Fig. 1. Sketch of the pump–probe imaging system. BS, beam splitter; M, ultrafast mirror.

Fig. 2. Morphology of three types of shockwaves induced by fs laser single pulse irradiation on PMMA surface with laser fluence of 11.9 J/cm² at a probe delay of 16 ns. HSW1, HSW2, and CSW are the three types of shockwaves, which represent the HSW in air, the HSW in the sample, and the CSW in the sample, respectively. The solid arrows depict the propagation direction of each shockwave. The dashed line indicates the contour of HSW2.

the localized temperature and pressure expanding both outside and inside the material. The atmosphere outside the sample was suddenly interrupted and compressed by the intense plasma, generating HSW1, as shown in Fig. 2. Inside the PMMA sample, extremely high gradients of pressure and temperature were also generated between the excited surface and the undisturbed bulk material due to strong ionization. Thus, a pressure wave formed and propagated into the sample in the form of HSW2[19], increasing the density of the surrounding material. The generation of a CSW because of the long Rayleigh length of the spatial-shaped Bessel pulse and the intense ionization along the focus region was reported in our previous study[18]. In this Letter, the Rayleigh length of the applied Gaussian pulse was much shorter than that of the Bessel pulse. However, the Gaussian beam was still guided into PMMA through the dynamical balance of self-focusing and defocusing because of the nonlinear properties of PMMA. FLs, the dark ionized linear range in the axis of the CSW, were then generated along the propagation of the beam inside PMMA. The intensive electron plasma in the linear range compressed the material fiercely to the surroundings, and the radial CSW was generated and expanded perpendicularly to the laser propagation direction.

Figure 3(a) displays the experimental results of the three types of shockwaves evolution with probe delay induced by single pulse irradiation with fluence of 11.9 J/cm². The initial HSW1 expanded acutely with a sharp increase of the localized temperature and pressure

Fig. 3. (a) Propagation distance of HSW1, HSW2, and CSW as a function of probe delay after single pulse irradiation with laser fluence of 11.9 J/cm². (b) Propagation distance of HSW1, HSW2, and CSW as a function of the pulse number with laser fluence of 11.9 J/cm²; the probe delay of HSW1 and HSW2/CSW is 1 and 16 ns, respectively.

after laser pulse irradiation. With increasing probe delay, the temperature and pressure within HSW1 tended to be stable. The expansion speed of the HSW1 front declined acutely with the probe delay and gradually slipped to a constant value of approximately 2.1 km/s from 32 km/s at the beginning. Although the morphology of HSW2 was similar to that of HSW1, the propagation characteristic of HSW2 was quite different from that of HSW1 in air, which was mainly determined by the nature of the sample. The result in Fig. 3(a) demonstrated that HSW2 expanded nearly at a constant speed of approximately 2.9 km/s, which was slightly higher than the sound speed in PMMA (∼2.6 km/s). CSW was induced by the ionization of FLs inside PMMA, which were several times longer than the Rayleigh length of the applied Gaussian laser pulse. The FLs first penetrated into the material and induced intensity ionization in the linear zone with about 100 μm in length (see Supplementary Material). After ionization, the linear zone expanded in the radial direction with a constant velocity of 5.2 km/s (two times the velocity of sound in PMMA, concerning twice the radius velocity). However, in Bessel beam ablation, CSW was induced by FLs that were directly ionized by the laser pulse, although the expansion velocities of CSW, depending on the nature of the material, were the same in both cases.

Figure 3(b) depicts the evolutions of the three shockwaves with the pulse number when 10 pulses were applied in order. The laser fluence of each pulse was 11.9 J/cm². In order to demonstrate the dynamics of HSW1 more effectively, the data of HSW1 in Fig. 3(b) was selected at a probe delay of 1 ns due to the stronger expansion of HSW1 at 1 ns, as shown in Fig. 3(a). The propagation distance of the HSW1 front decreased with the applied pulse number, and this decreasing trend was also confirmed at a probe delay of 16 ns. The flat surface was destroyed after the first pulse illumination, and the quality of the crater deteriorated with repeated ablation by subsequent pulses[20]. The rough morphology of the structure prevented the absorption of pulse energy through disordered scattering, leading to the decrease of the ionization intensity. Furthermore, the progressively rough and tapered wall of the structure obstructed the outward diffusion of the plasma/shockwave. The front of HSW2 was nearly in a linear relationship with the pulse number. With the ablation depth deepening with the pulse number (see Supplementary Material), the material density and the refractive index around the pre-ablated structure increased within the hemispherical volume by the stress of HSW2. However, the radial expansion distance of the CSW was almost constant with different pulse numbers and laser fluences (see Supplementary Material). These above characteristics of shockwave evolution with pulse numbers in Fig. 3(b) were universal for all of the probe delay in our Letter. Note that the CSW disappeared after 10 pulses ablation. Thus, the corresponding data point in Fig. 3(b) was absent. The reason for this phenomenon is discussed as follows.
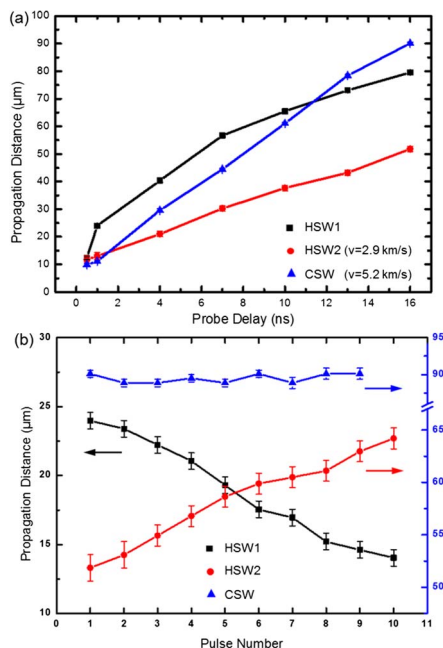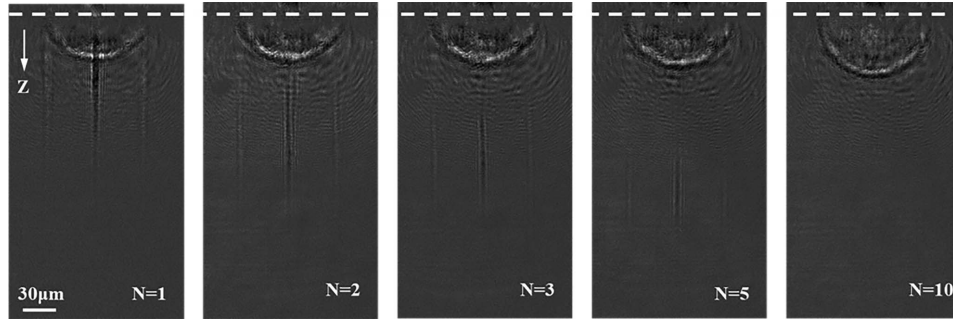
Fig. 4. CSW evolution with pulse number N. All shadowgraphs were captured at the same position with laser fluence of 11.9 J/cm^2 at a probe delay of 16 ns. The dashed line represents the surface of the sample and laser propagated from air in the Z direction.

The detailed characteristic evolution of CSWs with a pulse number is shown in Fig. 4 with laser fluence of 11.9 J/cm^2 at a probe delay of 16 ns. Although the radial expanding distance was almost unchanged between the pulses, the FLs (dark linear range) moved downstream in the Z direction and degenerated with increased pulse numbers. The ionization front induced by the fifth pulse (sub-graph $N = 5$ in Fig. 4) was approximately 50 μm deeper than that induced by the first pulse (sub-graph $N = 1$ in Fig. 4). The material removal was not responsible for this phenomenon because the crater depth after five pulses ablation was measured to be less than 10 μm (see Supplementary Material). Moreover, the length of the ionization channel became shorter with the pulse number (approximately 122 μm for $N = 1$ and 67 μm for $N = 5$) and totally vanished when pulse number was $N = 10$. Although the radial expanding features were constant with pulse number, the experimental results in Fig. 4 illustrated that the dynamics of FLs evolved both in length and intensity with multiple pulses.

The formation mechanism of FLs in transparent material can be attributed to the effect of self-focusing or spherical aberration[21], as discussed in previous studies. Self-focusing occurs when high intensity fs laser interacts with nonlinear dielectric material. FLs were the result of the dynamical balance of self-focusing and defocusing effects. Spherical aberration was induced by the refractive index difference of two different materials through which the laser passes. Thus, spherical aberration can be excluded from the filamentation mechanism, as the laser was focused on the surface of the sample in this Letter, and the nonlinear effect dominated the generation of FLs in this study. When a fs laser pulse illuminated the flat surface of the PMMA sample, refractive index n of the surface was changed by nonlinear absorption of pulse energy. The refractive index can be identified as

$$n = n_0 + n_2 I, \tag{1}$$

where n_0 is the linear refractive index, n_2 is the nonlinear refractive index ($\propto \chi^{(3)}/n_0^2$, where $\chi^{(3)}$ is the third-order nonlinear coefficient), and I is the laser intensity. For the PMMA sample, n_0 and n_2 were approximately 1.49 and 10^{-18} m^2/W, respectively[22]. The Gaussian

distribution of laser intensity led to the progressive decrease of the refractive index change Δn ($n_2 I$) in the radial direction. In the center of the focal point, the refractive index increased significantly ($\Delta n_{\max}$) due to the strong laser intensity. The refractive index change around the rim of the focal point ($\Delta n_{\min}$) was less than that of the center area. The radial descending refractive index distribution can be regarded as a convex lens, which can focus the beam into PMMA. Therefore, the beam near the center γ_2 was guided to F_1, and the marginal beam γ_1 was guided to F_2. With sufficient laser intensity, FLs were generated within the focal range $F_1 F_2$ by different focus positions of the beam due to the gradually varied refractive index, as qualitatively shown in Fig. 5(a).

When subsequent pulses were applied, the structure induced by previous pulses resisted the laser pulse propagating to the bottom of the crater. The laser intensity on the crater surface was lower than that of the flat surface with the first pulse. According to Eq. (1), the refractive index change $\Delta n'$ was less than the Δn induced by the first pulse. Moreover, the energy deposition and intensity of ionization decreased due to the rough surface topography of the crater, as mentioned previously. The ejection of
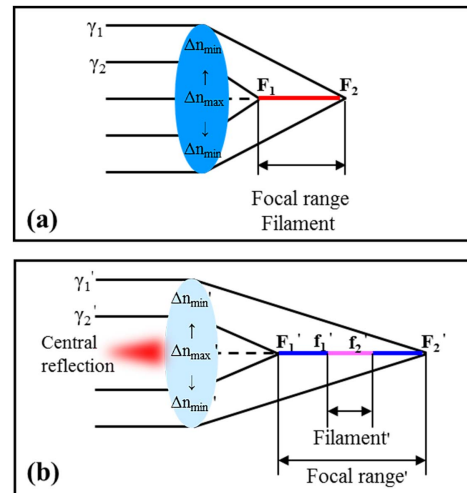

Fig. 5. Schematic diagram of the focal range and FL generation when (a) the first pulse is focused on the flat surface and (b) the subsequent pulse is irradiated on the pre-ablated structure.

electron plasma consequently debilitated with pulse number. Concerning these factors, the nonlinear effect was attenuated with the pulse number due to refractive index change $\Delta n'$, as schematized in Fig. 5(b). In other words, the theoretical focal range $F'_1 F'_2$ was elongated to downstream due to the decreasing focusing capability. However, the peak power of the marginal beam γ'_1 decreased below the critical power for self-focusing with the block of the pre-ablated structure. The head of the FL $f'_2 F'_2$ toward the output surface was invisible when the beam power was below the self-focusing threshold. The center reflection by the crater was the other reason for the shortening of the FL. As reported in a previous study[16], the reflection intensity reached the peak in the center range of the crater. The energy loss of reflection in the center area accounted for the degeneration of FL $F'_1 f'_1$ toward the input surface. Consequently, FLs generated by subsequent pulses were shorter and weaker, although the theoretical focal range was elongated downstream. Correspondingly, CSW induced by FLs was shortened and moved to the output surface, which finally vanished with 10 pulses, as depicted in Fig. 4. In conclusion, the decrease of refractive index change and insufficient peak power on the margin and center of the focal point dominated the attenuation of FLs, both in intensity and length with multiple pulses.

In this study, an ultrafast pump–probe shadowgraphs imaging technique was applied to investigate the three types of simultaneous shockwaves in PMMA induced by fs laser single/multiple pulses. With laser focusing on the sample surface, the evolution characteristics of these three shockwaves were indicated and analyzed with probe delay and pulse number. The structure ablated by pre-pulses had a negative effect on pulse energy deposition and suppressed the plasma expansion outside the sample. The generation of a CSW indicated that the energy of the Gaussian beam can be deposited deep inside the material beyond the Rayleigh length through filamentation. Although the expanding distance of the CSW was constant between pulses, the FLs in the center of the CSW moved downstream toward the output face and degenerated with pulse number. This phenomenon was attributed to the decreasing refractive index change and the self-focusing ability induced by degraded nonlinear effects. The pre-ablated structure of previous pulses had a negative effect on self-focusing of FLs due to suppressed laser intensity and refractive index change. The degraded laser intensity on the margin of the structure and the reflected beam in the center of focal point were responsible for the shortening of FLs on both ends due to insufficient peak power for self-focusing. Therefore, the CSW finally disappeared with 10 pulses. The experimental results and mechanism

revealed in this study illustrated that energy deposition was suppressed by a degraded nonlinear effect due to the pre-ablated structure in multiple pulses irradiation and facilitated the comprehension of highly efficient fs multiple pulses fabrication.

References

1. A. Stone, H. Jain, V. Dierolf, M. Sakakura, Y. Shimotsuma, K. Miura, and R. Kashyap, Sci. Rep. **5**, 10391 (2015).
2. Y. Li, W. Watanabe, K. Yamada, T. Shinagawa, K. Itoh, J. Nishii, and Y. Jiang, Appl. Phys. Lett. **80**, 1508 (2002).
3. B. Xia, L. Jiang, X. Li, X. Yan, W. Zhao, and Y. Lu, Appl. Phys. A **119**, 61 (2015).
4. J. Qiu, K. Miura, H. Inouye, J. Nishii, and K. Hirao, Nucl. Instrum. Methods Phys. Res. Sec. B: Beam Interact. Mater. Atoms **141**, 699 (1998).
5. C. M. B. Ho, S. H. Ng, and K. H. H. Li, Lab Chip **15**, 3627 (2015).
6. L. Jiang, A. D. Wang, B. Li, T. H. Cui, and Y. F. Lu, Light: Sci. Appl. **7**, 17134 (2018).
7. X. Sun, D. Cui, Y. Hu, D. Chu, G. Chen, J. Yu, and J. A. Duan, Chin. Opt. Lett. **16**, 101402 (2018).
8. Y. Zhang, R. M. Lowe, E. Harvey, P. Hannaford, and A. Endo, Appl. Surface Sci. **186**, 345 (2002).
9. D. Chu, K. Yin, X. Dong, Z. Luo, Y. Song, and J. A. Duan, Chin. Opt. Lett. **16**, 011401 (2018).
10. L. Jiang, P. Liu, X. Yan, N. Leng, C. Xu, H. Xiao, and Y. Lu, Opt. Lett. **37**, 2781 (2012).
11. D. Chu, X. Sun, Y. Hu, X. Dong, K. Yin, Z. Luo, and J. A. Duan, Chin. Opt. Lett. **15**, 071403 (2017).
12. Q. Xie, X. Li, L. Jiang, B. Xia, X. Yan, W. Zhao, and Y. Lu, Appl. Phys. A **122**, 136 (2016).
13. A. M. Alshehri and V. R. Bhardwaj, Opt. Mater. **62**, 512 (2016).
14. R. R. Gattass and E. Mazur, Nat. Photon. **2**, 219 (2008).
15. S. Sowa, W. Watanabe, J. Nishii, and K. Itoh, Appl. Phys. A **81**, 1587 (2005).
16. Q. Wang, L. Jiang, J. Sun, C. Pan, W. Han, G. Wang, and Y. Lu, Photon. Res. **5**, 488 (2017).
17. X. Zeng, X. Mao, S. B. Wen, R. Greif, and R. E. Russo, J. Phys. D: Appl. Phys. **37**, 1132 (2004).
18. G. Wang, Y. Yu, L. Jiang, X. Li, Q. Xie, and Y. Lu, Appl. Phys. Lett. **110**, 161907 (2017).
19. M. Sakakura, M. Terazima, Y. Shimotsuma, K. Miura, and K. Hirao, Opt. Express **15**, 5674 (2007).
20. F. Baset, A. Villafranca, J. M. Guay, and R. Bhardwaj, Appl. Surf. Sci. **282**, 729 (2013).
21. Q. Sun, H. Jiang, Y. Liu, Y. Zhou, H. Yang, and Q. Gong, J. Opt. A: Pure Appl. Opt. **7**, 655 (2005).
22. R. Osellame, G. Cerullo, and R. Ramponi, *Femtosecond Laser Micromachining: Photonic and Microfluidic Devices in Transparent Materials* (Springer, 2012).